CHEMICAL ENGINEERING TRANSACTIONS
VOL. 67, 2018
A publication of AIDIC
The Italian Association of Chemical Engineering
Online at www.aidic.it/cet
Guest Editors: Valerio Cozzani, Bruno Fabiano, Davide Manca

ISBN 978-88-95608-64-8; **ISSN** 2283-9216
DOI: 10.3303/CET1867003

Evaluation of Cyclic Corrosion on ASTM A335 P92 Steel Exposed to a Combustion Atmosphere in a Horizontal Boiler

Juan Orozco[a], Anibal Alviz-Meza[a,*], Viatcheslav Kafarov[a], Dario Y. Peña-Ballesteros[b], Camilo Osses[a], Maria Pinto[a]

[a]Centro de Investigación para el Desarrollo Sostenible en Industria y Energía, Universidad Industrial de Santander, Bucaramanga, Colombia. Ciudad Universitaria, Cr 27 #9, A.A. 680002
[b]Grupo de Investigación en Corrosión, Universidad Industrial de Santander, Bucaramanga, Colombia. Parque Tecnológico Guatiguará, Piedecuesta, A.A. 681011
anibalalvizm@hotmail.com

The use of industrial boilers for steam generation at industrial level is carried out under high temperature conditions, generating potentials corrosive atmospheres composed by CO_2, N_2, O_2 and H_2O; causing the deterioration and wastage of steels mechanical properties in equipment, as well as large economic losses. In this research work, the high temperature corrosive behavior of ASTM A335 P92 steel exposed to a real combustion environment in a horizontal pirotubular boiler was evaluated. Through characterization techniques such as: X-Ray Diffraction (XRD), X-ray Photoelectron Spectroscopy (XPS), Scanning Electron Microscopy (SEM) and X-ray Dispersive Energy (EDX), the morphology of the oxide layer formed, and its corrosion products were obtained. For its part, the gravimetric technique was used to analyze the kinetic corrosion behavior of the alloy, due to the mass gain per unit area against the testing times 24, 48, 120, 240 and 360 h. These results lead to determinate the corrosion rate and the kinetic constant according to the oxide parabolic growth law. Finally, it is concluded that ASTM A335 P92 steel is an alloy of potential use in combustion environments, where it has shown an outstanding behaviour respect to cyclical thermal processes at high temperatures. However, the limitation of this study is represented in the short testing times.

1. Introduction

Boilers are widely used in the refinery industry, and their operation is greatly influenced by different constant fluctuations such as: working conditions and chemical composition of the fuel used to achieve high temperatures. According to Kafarov et al. (2015), the increase in temperature in combustions environments can cause serious problems of corrosion in the boilers' components; as is the case of super heater tubes and steam generators. Another complement study developed by Alviz et al. (2017), indicates that high temperatures in combustion processes can reduce the physical properties of involved alloys, leading to equipment failures and considerable economic losses due to unexpected stops in production and maintenance.

On the other hand, regarding to the type of energy source used in equipment such as furnaces and boilers, Ayala et al. (2014) promotes the use of natural gas as a less corrosive energy source, since highly corrosive compounds such as H_2S can be suppressed; effect favoured by refinery gases. In a combustion environment generated by the burning of natural gas with air in excess, typically, it is feasible to obtain an atmosphere rich in CO_2, O_2, N_2 and H_2O, where the simultaneous effects of nitridation, carburization and oxidation could coexist. The oxidation phenomenon is the most important of those previously described, according to Orozco et al. (2017) the ferritic ASTM A335 P92 (P92) steel can generate an adherent and continuous superficial layer rich in chrome, which can avoid the participation of other corrosive phenomena such as carburization, reducing the deterioration of the alloy physical properties.

For its part, P92 steel belongs to the ferritic steels family, which are a series of alloys that have excellent structural properties thanks to the addition of elements such as V, Mo, Nb and W, which can withstand aggressive chemical conditions in equipment, as point out Barbadikar et al. (2015). Finally, the objective of

Please cite this article as: Orozco J., Alviz Meza A., Kafarov V., Peña Ballesteros D.Y., Osses C., Pinto M., 2018, Evaluation of cyclic corrosion on astm a335 p92 steel exposed to a combustion atmosphere in a horizontal boiler, Chemical Engineering Transactions, 67, 13-18
DOI: 10.3303/CET1867003

this research work was to evaluate P92 steel behavior in a typical combustion environment of a boiler, to promote a little more its use, considering that it is a low-cost alloy with respect to stainless steels.

2. Materials and methods

The applied methodology in this research work was like one used by Alviz et al. (2017) to study corrosion in a real combustion refinery environment. The development of this work had an experimental and a simulation part, where simulation was useful to predict the possible corrosion products.

The first step to simulate theoretical corrosion products was to obtain the combustion gases composition through Aspen HYSYS 8.6 software. Additionally, once having the experimental conditions, the composition of steel and combustion gases, to determine the theoretical corrosion products with HSC Chemistry 5.1 software was possible.

Regard to experimental part, the boiler used for this corrosion study has a cyclic functioning, alternating between 12 h of continuous operation and 12 h out of service. This type of experimental conditions, typically correspond to studies of cyclic corrosion, because temperature does not remain uniform with time. Table 1 and Table 2 show another operating variables of the boiler, while Table 3 shows the elemental weigh fraction of the studied alloy.

Table 1: Boiler operating variables

Energy source	Air in excess	Operating pressure	Volumetric flow	Temperature
Natural gas	12 %	5.8 atm	24 m^3/h	850 ºC

Table 2: Molar natural gas composition used by the boiler

Compounds	CO_2	N_2	CH_4	C_2H_6	C_3H_8	i-C_4H_{10}	n-C_4H_{10}	i-C_5H_{12}	n-C_5H_{12}
%Molar	1.827	0.476	89.076	5.636	1.945	0.395	0.345	0.225	0.075

Table 3: Elemental weigh fraction of P92 steel

%Mo	%C	%Si	%Mn	%P	%W	%Ni	%Cr	%V	%Nb	%Al	%N	%Fe
0.420	0.115	0.220	0.454	0.013	1.979	0.119	9.140	0.115	0.055	0.011	0.039	87.320

About the selected exposure times, given the equipment operation, the implemented times were 24, 48, 120, 240 and 360 h. This means that in this work only the initial corrosive effects developed on P92 steel, in a real combustion environment, were studied. To introduce P92 samples in the boiler a coupons holder was use; in Figure 1 is possible to observe its disposition inside the boiler.

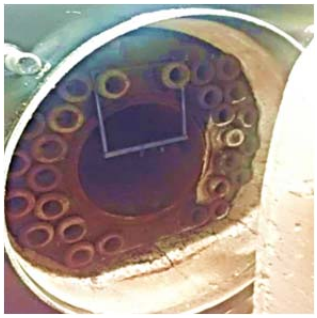

Figure 1: Back opening of the boiler, where the holder of the samples can be observed; which was in front of the flame zone

Regard to coupons preparation, through thread cutting technique, samples of 10 mm long, 15 mm high and 2 mm wide, were obtained. These samples were sanded before testing from SiC sandpaper No. 180 to 600. Each coupon was subjected to ultrasonic cleaning in acetone during 10 min, dried and marked, as is recommended by standard ASTM G1 (ASTM, 2011). To characterize the results XPS, SEM-EDS, XRD, hardness, microhardness and optical microscopy techniques were applied. Finally, the kinetic study was carried out considering the dimensions of the coupons, as well as the mass gained by each one.

3. Results

3.1 Theoretical corrosion products

The theoretical combustion gases were simulated in Aspen HYSYS 8.6 software, taking into account the natural gas composition data and the percentage of excess air, previously detailed in Tables 1 and 2. The high percentage of free oxygen in the simulated combustion environment is an important result to highlight, as is shown in Table 4.

Table 4: Molar combustion gases composition

Compounds	CO_2	N_2	O_2	H_2O
%Molar	8.30	72.73	3.37	15.60

Thermodynamic equilibrium was calculated using the experimental conditions of pressure and temperature, as well as the steel and combustion gases composition. This simulation gave the theoretical corrosions products, which can be observed in Figure 2. The molar steel/gas ratio used for this simulation in HSC Chemistry 5.1 was 1/1000, as is recommended by John (2010).

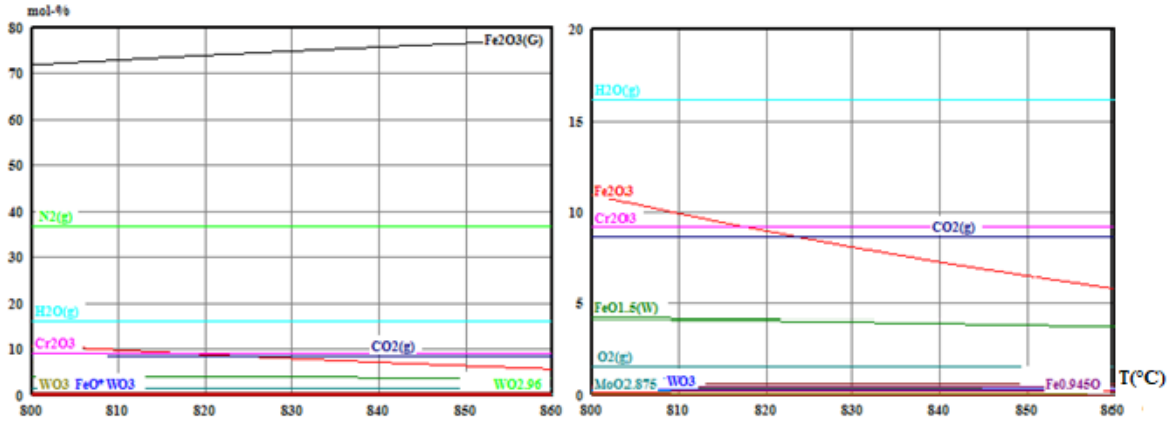

Figure 2: Variation of the Molar percentage from the simulated corrosion products against temperature

The main result of the simulation showed that, for the selected experimental conditions, carburization is not thermodynamically favoured, but oxidation does. The predominant oxides identified were: hematite and chromite, as well as tungsten and molybdenum oxides. These results can be explained by the high oxygen potential in the environment, which can suppress carbides formation.

3.2 Microanalysis of Scanning Electron Microscopy with Energy Dispersive X-ray (SEM-EDX)

Figure 3 reveals the morphology of the oxide layer deposited on the P92 steel after 360 h of cyclic corrosion. The presence of two layers is observed, one represented by zone 1 and another by zone 2. Zone 2 corresponds to an internal layer with an average thickness of 37.59 µm, and constituted mainly by chromium, oxygen and iron. While zone 1 corresponds to the outer layer, with a thickness of approximately 46.63 µm and composed mainly of iron. Additionally, it can be said that oxide morphology has an acceptable appearance, considering the cyclic corrosion process and the high temperature to which the alloy was subjected. Said morphology is probably the reason because the carburization phenomenon was not identified, also considering the high oxygen potential in the environment.

For longer exposure times, more defects are expected in the oxide layers, such as multiples pores, cracks and voids. Which by increasing their size and quantity favour their coalition and final detachment of zone 1 or a large part of it, allowing the diffusion of carbon to the metal matrix. This effect called internal carburization tends to affect the ductility of the steel, until generating cracks and fissures in it, ending with its useful life period.

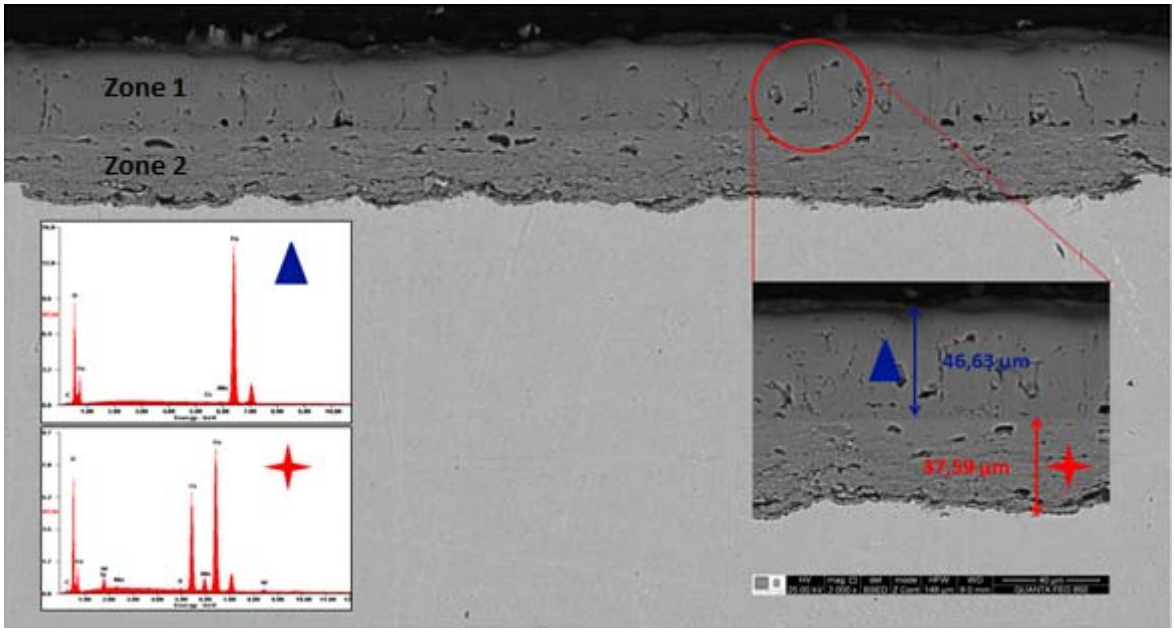

Figure 3: SEM-EDS from P92 sample after 360 h at 850 ºC

3.3 Analysis of X-ray Photoelectron Spectroscopy (XPS)

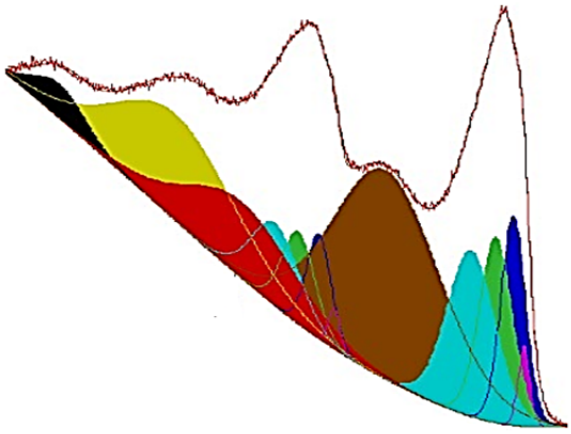

Name	Pos.	FWHM	L.Sh.	Area	%Area
Fe 2p 3/2	709.94	2.003	GL(30)	27869.7	6.729
Fe 2p 3/2	709.20	0.951	GL(30)	5081.1	1.227
Fe 2p 3/2	711.15	2.696	GL(30)	33241.7	8.026
Fe 2p 1/2	723.45	2.003	GL(30)	13934.9	3.360
Fe 2p 1/2	724.86	2.696	GL(30)	16620.9	4.008
Fe 2p	733.40	9.958	GL(30)	70391.7	16.957
Fe 2p	741.49	4.294	GL(30)	9843.0	2.369
Fe 2p 1/2	722.39	0.951	GL(30)	2540.6	0.613
Fe 2p	718.76	8.998	GL(30)	1246119	30.064
Fe 2p 3/2	712.86	3.929	GL(30)	43272.8	10.446
Fe 2p 1/2	726.46	3.929	GL(30)	21636.4	5.216
Fe 2p	728.81	8.963	GL(30)	45577.8	10.985

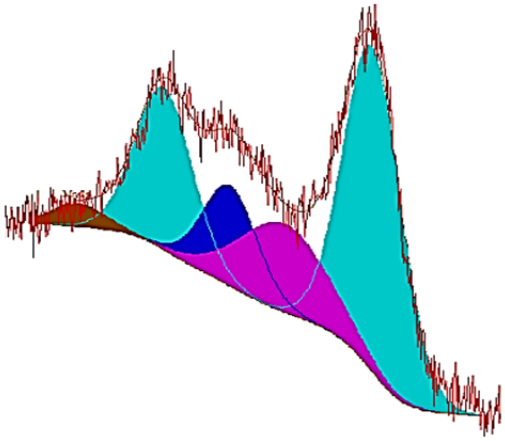

Name	Pos.	FWHM	L.Sh.	Area	%Area
Mn 2p 1/2	641.44	3.744	GL(30)	9798.7	44.914
Mn 2p 3/2	653.04	3.744	GL(30)	4899.4	22.441
Mn 2p	649.35	3.555	GL(30)	2887.7	12.212
Mn 2p	646.33	5.826	GL(30)	4166.7	17.624
Mn 2p	657.82	3.574	GL(30)	664.6	2.809

Figure 4: Fe 2p and Mn 2p region studied by XPS

For the measurements, a monochromatic Al Kα X-ray source operated at 100 W was used. The spectrometer pass energy was fixed at 20 eV, and the estimated overall instrumental broadening was around 0.5 eV. The regions selected taking into account the elements identified in zone 1 by EDS were: C 1s, O 1s, Fe 2p, Cr 2p and Mn 2p. Finally, the energy was calibrated by setting the adventitious C 1s peak to 284.8 eV.

For Fe 2p fitting a methodology like one used by Sanchez et al. (2017) was applied, who made their deconvolution by multiple peaks. The presence of hematite was confirmed on the surface, considering the shape of Fe 2p and the position of Fe 2p3/2 at ~710.4 eV. Additionally, the existence of a peak at ~719 eV is a typical fingerprint that corroborates its presence. The formation of magnetite is not likely due to the absence of its characteristic shoulder at ~709 eV, and to the thickness of the hematite layer. The above is confirmed by XRD results, where hematite is identified, which speaks very well about the thickness of this layer. Finally, the thermodynamic equilibrium also promotes hematite formation on the surface oxide layer, as it was shown in the simulation.
On the other hand, in the region of Mn 2p, the presence of Mn_xO_{x+1} was identified at ~741.4 eV. The presence of chromite could not be confirmed on the surface oxide layer; by the little or no evidence of chromium in it, as EDX results indicate. According to this superficial analysis, no external carburization was identified.

3.4 X-Ray Diffraction (XRD) analysis

Through x-ray diffraction analysis, the crystalline structures present in the oxide layer were determined, after 360 h of testing. So, it was identified: Hematite (α-Fe_2O_3), Magnetite (Fe_3O_4) and Wustite (FeO). These results are consistent with EDX and XPS results. These results also rule out a possible internal carburization.

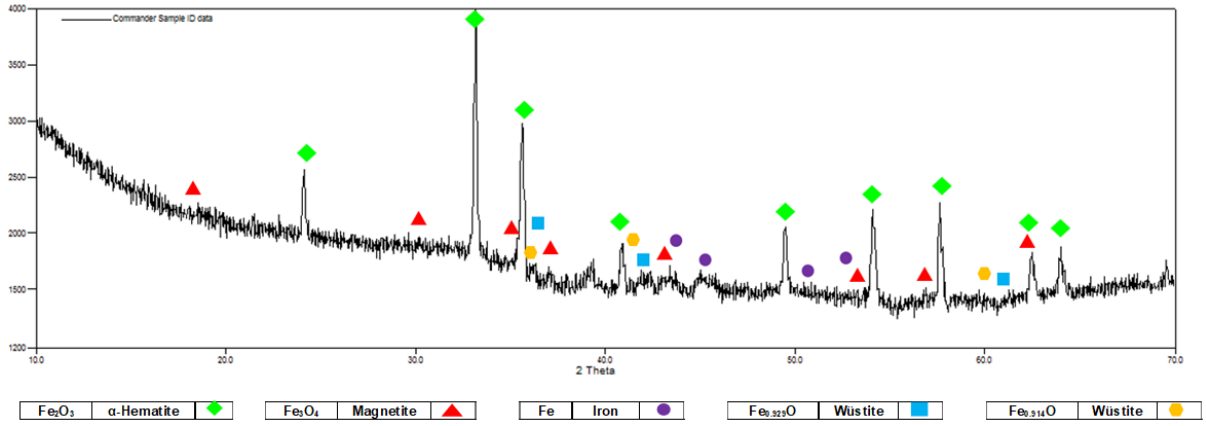

Figure 5: X-ray diffraction analysis of surface sample submitted to 360 h of cyclical corrosion

3.5 Kinetic Study

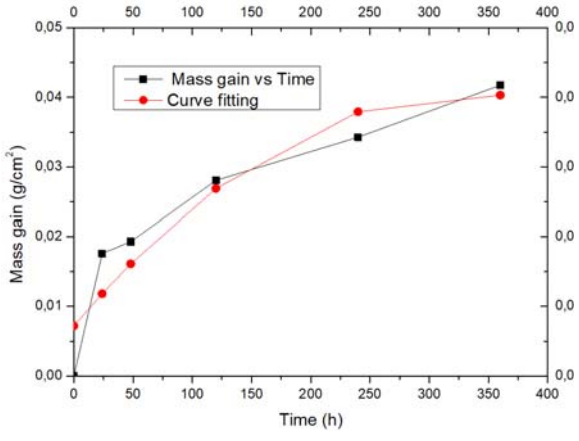

Figure 6: P92 mass gain against testing times

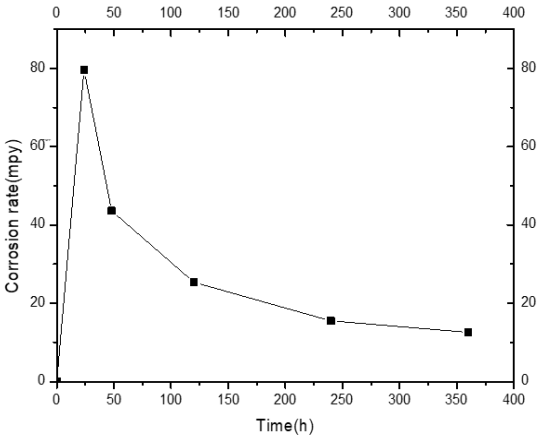

Figure 7: Corrosion rate against testing times

In Figure 6 it is observed that the mass gain curve has a parabolic behavior, giving the kinetic constant $K_p = 3x10^{-7}\ g^2cm^{-4}h$, which is mainly related with the high diffusion of chromium to form homogenous and compact surface layers of protective internal oxides. This fact can be corroborated with the corrosion rate in

Figure 7, where, as time passes the corrosion rate decreases, which indicates that P92 steel is being protected against corrosion. The corrosion rate (R_{corr}) was determined using Eq (1).

$$R_{corr} = \frac{K}{\rho * A} * \frac{\Delta W}{t} \quad (1)$$

Where, K is the constant kinetic, ρ is the alloy density, A is the reaction area, t is time, and ΔW the mass gain. As is shown in Figure 7 the corrosion rate is not directly proportional to time, having a maximum value of 79.56 mpy at 24 h. After 24 h it is possible to identify three intervals: in the 24 to 48 h interval the corrosion rate decreases by 55% with respect to its initial value, from 48 to 120 h there is a decrease of 83 %, and finally for the interval of 120 to 360 h the minimum value of 12.58 mpy is reached. In this way, it is verified that as time passes, P92 steel is being protected by an oxide layer, where the diffusive processes decrease over time.

4. Conclusions

Through this work it was possible to evaluate the behaviour of P92 ferritic steel in the cyclical combustion environment of an industrial boiler. By exposing this steel to temperature fluctuations between 25 and 850 °C, and for periods of time up to 360 h, it is possible to obtain a protective oxide layer. The value obtained for the kinetic constant K_p was $3x10^{-7}\ g^2cm^{-4}h$. Regarding the morphology of the oxide layer, it could be observed that it was made up of two zones; an internal one rich in chromium and an external one rich in iron. These results were useful for XRD and XPS analysis, where the presence of hematite, magnetite and chromite was mainly suggested, ruling out the presence of carburization according with simulation products. Finally, it is concluded that ASTM A335 P92 steel is a steel of potential use in combustion environments, where it has shown good behaviour with respect to cyclical thermal processes. However, the limitation of this study is represented in the short testing times.

Acknowledgments

The authors express their acknowledgments to the Administrative Department of Science, Technology and Innovation of Colombia (COLCIENCIAS) and Colombian Network of Knowledge in Energy Efficiency (RECIEE) for financial support of this work, that is part of the project “Consolidation of the knowledge network on energy efficiency and its impact on the productive sector under international standards - Design of a methodology for the eco-efficient management of combustion processes, case study: the oil refining industry” code of COLCIENCIAS: 110154332086.

References

Alviz, A., Kafarov, V., Meriño L., 2017, Methodology for evaluation of corrosion damage during combustion process in refinery and petrochemical industry. case study: AISI 304 and astm A335 P5 steels, Chemical Engineering Transactions, 61, 1315-1320.

American Society for Testing and Materials, 2011, Standard Practice for Preparing, Cleaning, and Evaluating Corrosion Test Specimens (ASTM G1-03 ed.). United States: ASTM International.

Aspen HYSYS (version 8.6) [software], 2014, obtained from <www.aspentech.com/en/resources/press-releases/aspentech-introduces-aspenonert-version-8-6-software2147490592>, 28-05-18.

Ayala B., Aparicio A., Garcia, E., 2016, Review of calculation of calorific value and dew point of natural gas, and estimating uncertainties. Revista ION, 29, 2, 85-97.

Barbadikar, D. R., Deshmukh, G. S., Maddi, L., Laha, K., Parameswaran, P., Ballal, A. R., Peshwe, D. R., Paretkar, R. A., Nandagopal, M., Mathew, M. D., 2015, Effect of normalizing and tempering temperatures on microstructure and mechanical properties of P92 steel, International Journal of Pressure Vessels and Piping, 132–133, 97–105.

HSC Chemistry (version 5.1) [software], 2002, obtained from <hsc-chemistry.software.informer.com/5.1/.>, 28-05-18.

John, R., 2010, Sulfidation and mixed gas corrosion of alloys. Shreir’s Corrosion, 240–271.

Kafarov, V., Toledo, M., Meriño, L., 2015, Numerical Simulation of Combustion Process of Fuel Gas Mixtures at Refining Industry, Chemical Engineering Transactions, 43, 1351–1356.

Orozco, J., Kafarov, V., Peña-Ballesteros, D., Alviz, A., 2017, Effects of oxidation-nitridation in the presence of water vapor on ASTM A335 P92 steel using SEM-EDS and XPS characterization techniques, IOP Conf. Series: Journal of Physics, 935, 1-7.

Sanchez, B., Huerta-Ruelas, J. A., Cabrera-German, D., Herrera-Gomez, A., 2017, Composition assessment of ferric oxide by accurate peak fitting of the Fe 2p photoemission spectrum, 49, 253-260.